

Full paper

Super-robust and frequency-multiplied triboelectric nanogenerator for efficient harvesting water and wind energy

Zhiming Lin^{a,b,c,1}, Binbin Zhang^{b,1}, Hengyu Guo^{b,1}, Zhiyi Wu^b, Haiyang Zou^b, Jin Yang^c, Zhong Lin Wang^{a,b,*}

^a Beijing Institute of Nanoenergy and Nanosystems, Chinese Academy of Sciences, Beijing, 100083, PR China

^b School of Materials Science and Engineering, Georgia Institute of Technology, Atlanta, GA, 30332-0245, USA

^c Key Laboratory of Optoelectronic Technology & Systems (Ministry of Education), Department of Optoelectronic Engineering, Chongqing University, Chongqing, 400044, PR China



ARTICLE INFO

Keywords:

Triboelectric nanogenerator

Pendulum

Super-robust and frequency-multiplied

ABSTRACT

Mechanical energy in ambient, such as water wave, wind, vibration, and human activities, is a green energy that is widely distributed and universally achievable. However, this type of energy has ultra-low frequencies and variable amplitudes, so it is rather challenging to collect them at high efficiency. Here we report a pendulum inspired triboelectric nanogenerator (P-TENG), which could not only boost the output frequency multiple times using a pendulum structure, but also hugely improve the harvesting efficiency through a transformation of impact kinetic energy into potential energy. The P-TENG also has ultrahigh sensitivity and active response to mechanical triggering from a random direction and superior durability for long time operation. A single trigger from the environment, the P-TENG shows a continuous electrical output for 120 s at a frequency of 2 Hz, and its output energy of which is 14.2 times larger than the energy of conventional free-standing TENG. Owing to the air gap between the triboelectric layer and electrodes and the mechanism of electrostatic induction, the P-TENG can work with little frictional resistance and surface wearing, largely enhancing its robustness and durability. The network of P-TENGs was successfully demonstrated to scavenge water wave or wind energy as sustainable power sources. Given the features of exceptional output performance, unprecedented robustness and universal applicability resulting from distinctive mechanism and structure, the P-TENG is a promising method to efficiently harvest energy from the ambient environment with possibility contributing to the blue energy.

1. Introduction

As the world moving toward the era of internet of things (IoTs) and artificial intelligence, abundant of sensing nodes are required to be integrated into the system [1–7]. Although the power required to drive a single sensor unit is very tiny, the number of such electronics in the sensor network is gigantically huge, around the range of trillions. In artificial intelligence, we inevitably have to consider human activities and interfacing human with machine, and human motion is an ideal source of energy for driving wearable electronics. Thus, harvesting energy from surroundings as sustained and self-sufficient power sources has been considered as an ideal solution for such sensing nodes, aiming at forming the self-powered sensing systems [8–11]. Extensive research efforts have been dedicated to the development of harvesting energy from our living environment, including thermal [12], solar [13],

biochemical [14] and mechanical [15]. Among them, harvesting the ambient mechanical energy has attracted long-lasting attentions for its universal availability and extensive green energy scales from tiny cells to oceanic waves [16–18].

Triboelectric nanogenerators (TENGs) have been proven as an effective technology for converting mechanical energy into electricity based on the coupling effect of the contact electrification and electrostatic induction, with unique features of high efficiency, high power density, light-weight, low cost, diverse material selectivity, simple design, and environmental friendliness [19–27]. Significant efforts have been made in the TENG for harvesting various kinds of mechanical energy including wind, body movement and ocean wave, etc [28–31]. Nevertheless, little work has ever been focused on the durability and stability of the TENG based device. The material abrasion makes the TENG nondurable for long-term service and ultra-low excitation

* Corresponding author. Beijing Institute of Nanoenergy and Nanosystems, Chinese Academy of Sciences, Beijing, 100083, PR China.

E-mail address: zhong.wang@mse.gatech.edu (Z.L. Wang).

¹ These authors contributed equally to this work.

frequency diminishes the energy harvesting efficiency. Although Lin et al. presented a rolling TENG with multiple steel rods to realize the improvement of the robustness and stability, there also exists friction between triboelectric layers, leading to energy loss and degradation of the surface morphologies due to the frictional force [32]. Furthermore, most of the mechanical energy in our surrounding exhibit at ultra-low frequencies, which contributes to the low energy conversion efficiency. Therefore, to utilize the ultra-low frequency excitation to achieve a high-frequency output is a great challenge.

Here, we developed a super-durable and frequency-multiplied TENG for efficient energy harvesting from water wave and wind energy. In the protocol, a single pendulum inspired TENG (P-TENG) operating at the free-standing mode is proposed. The TENG based on the pendulum structural design is capable of improving the output frequency (up to 2 Hz) at a low driving frequency, largely enhancing the output power. The awkward predicament of static charge dissipation in the free-standing model TENG is well resolved without compromising the device robustness by using thin strips as a triboelectric layer. The characteristic of aggregated TENG networks for harvesting blue energy and wind energy is demonstrated, which can be serviced as power sources for powering portable electronics and charging capacitors. Given the frequency-multiplied electric output and the superior device robustness, this work presents a method for TENGs to achieve high efficiency and stability for energy harvesting but also push the self-powered sensing system for large-scale applications.

2. Results

2.1. Structure and working principle

The 3D structural scheme of the pendulum inspired TENG (P-TENG) is illustrated in Fig. 1a. It consists of three parts, an electrode layer, a pendulum triboelectric layer, and thin stripes. The electrode layer contains an internal circular electrode (Electrode 1) and an external

ring electrode (Electrode 2) deposited onto the cambered acrylic. A layer of PTFE film acts as the dielectric layer covering the electrode layer. As for the pendulum triboelectric layer, a layer of copper film with the same dimensions of the internal circular electrode serves as the freestanding triboelectric layer, and there exists a free-standing gap (1 mm) between the pendulum triboelectric layer and the electrode layer, which is important for improving the degree of oscillation and reducing the materials abrasion. The pendulum triboelectric layer is connected to the outer acrylic spherical shell with a cotton thread for free oscillation. For the thin stripes, identical PTFE stripes with equal spacing were uniformly fixed onto the outer edge of the cambered acrylic as the charge pump. This configuration is extremely sensitive to external mechanical excitation, thus, a small disturbance will lead to a relatively large motion between the triboelectric layers. To enhance the triboelectric effect, microstructures were created on the surface of the PTFE by the inductively coupled plasma (ICP) etching treatment to promote the surface frictional effect. Scanning electron microscopy (SEM) image of the surface is displayed in the insert in Fig. 1a. The detailed experimental setup is described in the Experimental section, which is plain and compatible with mass production.

Relying on the unique conjugation between the tribo-electrification and electrostatic induction, the fundamental operation mechanism of the P-TENG is schematically depicted in Fig. 1d and e. Here, we define the stationary state that the pendulum stays at the middle without any excitation as the initial state, as shown in Fig. 1d(i). Assuming there exists no original charges on the surfaces of the triboelectric layers at the initial state. Once an external triggering is applied to the P-TENG, the pendulum triboelectric layer will naturally swing (to left part) with a large amplitude and then contact with the thin PTFE stripes slightly. According to the triboelectric series²³, the electrons will be transferred from the pendulum copper layer to PTFE stripes with a result that the PTFE is negatively charged while the pendulum copper is positively charged. Then pendulum triboelectric layer will swing rightward, and be tribo-electrified with the right-hand PTFE stripes, leading to a

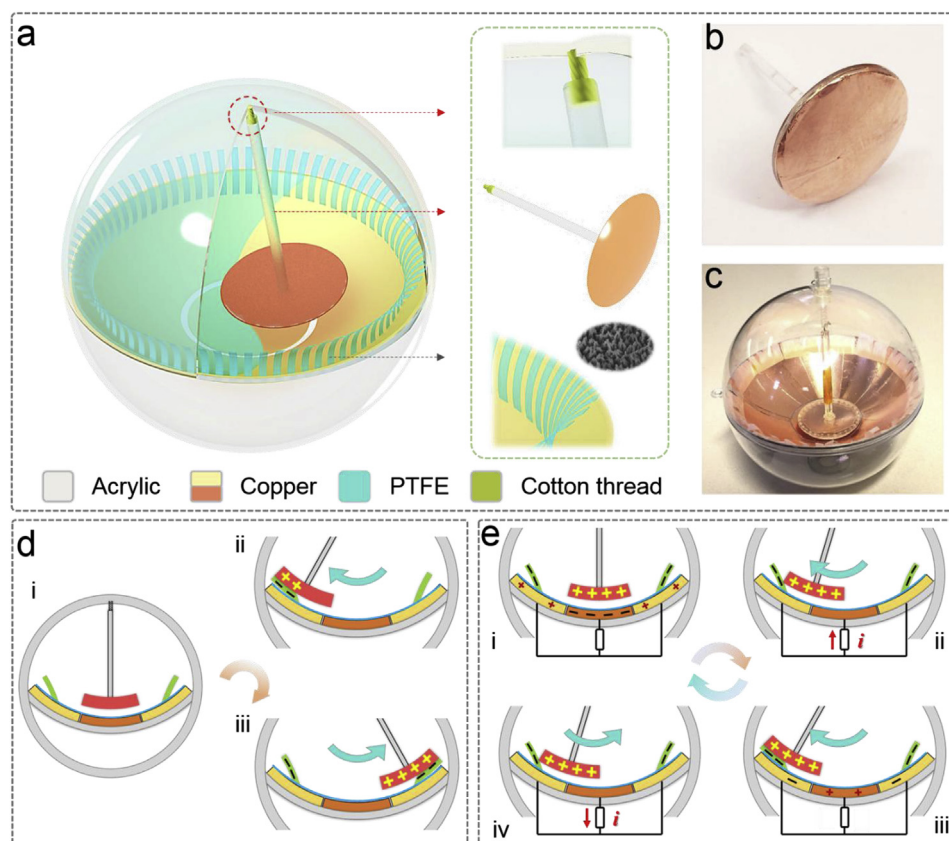


Fig. 1. Structural design and working principle of the P-TENG. (a) Schematic illustrations of the P-TENG, which has three parts, that is, an electrode layer, pendulum triboelectric layer, and thin stripes. The zoomed-in illustrations are the cotton thread, pendulum triboelectric layer, and thin stripes. (b) Photograph of a pendulum triboelectric layer. (c) Photograph of the as-fabricated P-TENG. Schematics of working principle of the P-TENG for (d) tribo-electrification process, and (e) electrostatic induction.

growing amount of positive charges on the pendulum copper layer. It can be seen that the PTFE stripes play a role of a charging pump in such a process.

At the initial state, as shown in Fig. 1e(i), ideally, equal amount of negative and positive charges on the electrodes will be induced to reach an electrostatic equilibrium. While an external vibration makes the pendulum triboelectric layer swing leftward Fig. 1e(ii) until reach the maximum amplitude Fig. 1e(iii). Similarly, the pendulum copper will induce negative charges at Electrode 2, the negative and positive charges will be redistributed on both Electrode 1 and Electrode 2 to achieve electrostatic equilibrium, according to the principle of the equipotential body, which drives the electrons flow from Electrode 1 to Electrode 2. Subsequently, the pendulum triboelectric layer swings backward and the electrons will flow back from Electrode 2 to Electrode 1 to balance the potential difference (Fig. 1e(iv)). As the pendulum triboelectric layer keeps moving rightward, similar electron flows can be produced between the electrodes, as depicted in Supplementary Fig. S1. Thus, alternating current in the external circuit can be produced via periodically swing of pendulum triboelectric layer. This is one cycle of the power generation process. It is noted that there exists no contact between the triboelectric layer and electrodes due to the free-standing gap except electrostatic induction process. Thus, little damage to the triboelectric layers ensures the durability of the materials, contributing to a time-lasting work of the P-TENG.

2.2. Pendulum model analysis

As is well-known, a pendulum consists of a mass m hanging from a string of length l and fixed at a pivot point. When displaced to an initial angle and released, the pendulum will swing back and forth with periodic motion, as shown in Fig. 2a. In our protocol, the point connected by a cotton thread can be regarded as the pivot, the length of the acrylic rod is served as the pendulum length. It should be specially explained that the pendulum triboelectric layer is a centrosymmetric structure, thus it can be considered as a mass point and the physical model can be classified as the simple pendulum model rather than a compound pendulum. By applying Newton's second law for rotational systems, the equation of frequency for a simple pendulum may be obtained

$$f = \frac{1}{2\pi} \sqrt{\frac{g}{l}} \quad (1)$$

According to equation (1), the frequency for a simple pendulum does not depend on the mass or the initial angular displacement but depends only on the length l of the rope and the value of the

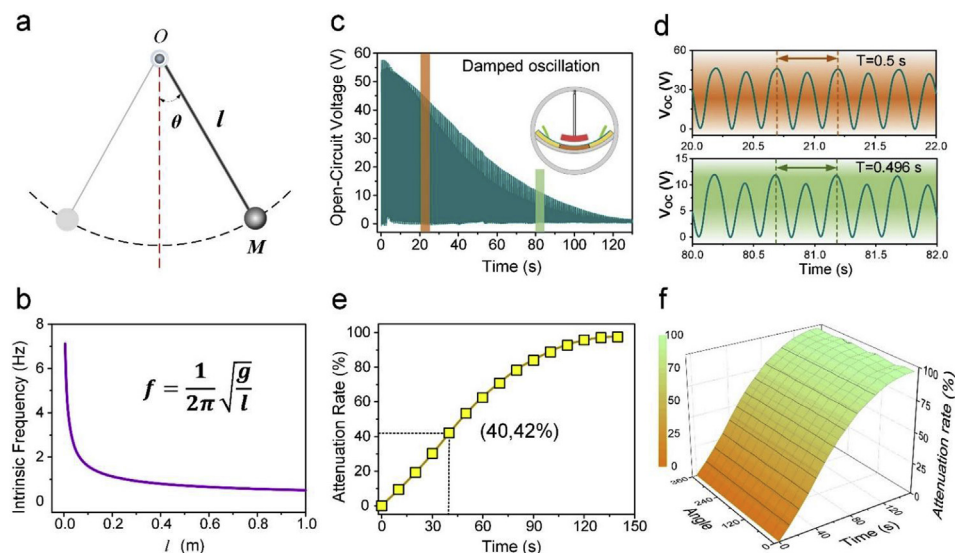


Fig. 2. Pendulum model analysis. (a) Schematic diagram of the pendulum model. (b) Simulated frequency of the pendulum as a function of length. (c) Open-circuit voltage of the proposed P-TENG for an external excitation. (d) Open-circuit voltages of the proposed P-TENG at the time of 20 s and 80 s. (e) Attenuation rate of the open-circuit voltage of the open-circuit voltage for an external excitation. (f) Attenuation rate of the open-circuit voltage at any excitation angles.

gravitational field strength g . Here, we simulated the frequency as a function of the length, as depicted in Fig. 2b ($g = 9.8 \text{ m/s}^2$). It shows that a smaller length contributes to a higher swing frequency, and the swing frequency significantly reduces as the length grows until the length grows to 0.1 m. In our design, a pendulum triboelectric layer with a length of 62 mm is adopted in the proposed P-TENG and the output frequency of which is predicted around 2 Hz. Fig. 2c and Supplementary Video S1 illustrate the open-circuit voltage of the proposed P-TENG after an external excitation. As the pendulum triboelectric layer swing back and forth, the amplitude of the pendulum triboelectric layer declines due to air friction, and we can see that it lasts more than 120 s until the triboelectric layer eventually comes to rest, rendering an outstanding frequency-multiplied performance. In the meantime, the output frequencies of the proposed TENG at the time of 20 s and 80 s remain unchanged (Fig. 2d), which is favorable consistent with the simulation result. Fig. 2e indicates that the attenuation rate of the open-circuit voltage decreases continuously due to the air friction, and which reaches to 42% (32.6 V) after 40 s, showing a long-time effective output performance. Furthermore, the attenuation rate of the open-circuit voltage for different excitation directions were also investigated systematically, as illustrated in Fig. 2f. The attenuation rates at different angles indicate a complete consistency, which is beneficial from the pendulum model for the free motions at an arbitrary angle in space.

Supplementary video related to this article can be found at <https://doi.org/10.1016/j.nanoen.2019.103908>.

2.3. Comparison of the P-TENG and in-plane TENG

To demonstrate the high-efficiency of energy harvesting of the P-TENG, a typical in-plane TENG with the same diameter of the P-TENG was also studied for comparison, as demonstrated in Fig. 3a, e. In the free-standing triboelectric mode, a layer of copper film direct contact with the triboelectric layer, resulting in frictional resistance as it slides, in which case there is not air gap. Fig. 3b, f show the open-circuit voltages of the two TENGs as they were applied an external trigger every 120 s. The output performance of the P-TENG can last 120 s with the output frequency of 2 Hz, but the conventional free-standing TENG only have a single open-circuit voltage output with the value of 360 V (Fig. S2 also depicts the output performances of conventional free-standing TENG for the charging accumulation process). Similar to the open-circuit voltage, the short-circuit current of the P-TENG decrease gradually, and the current of conventional TENG just presents one-time instantaneous output. The frequency-multiplied output performance of the P-TENG has 480 cycles output, which is attributed to the pendulum

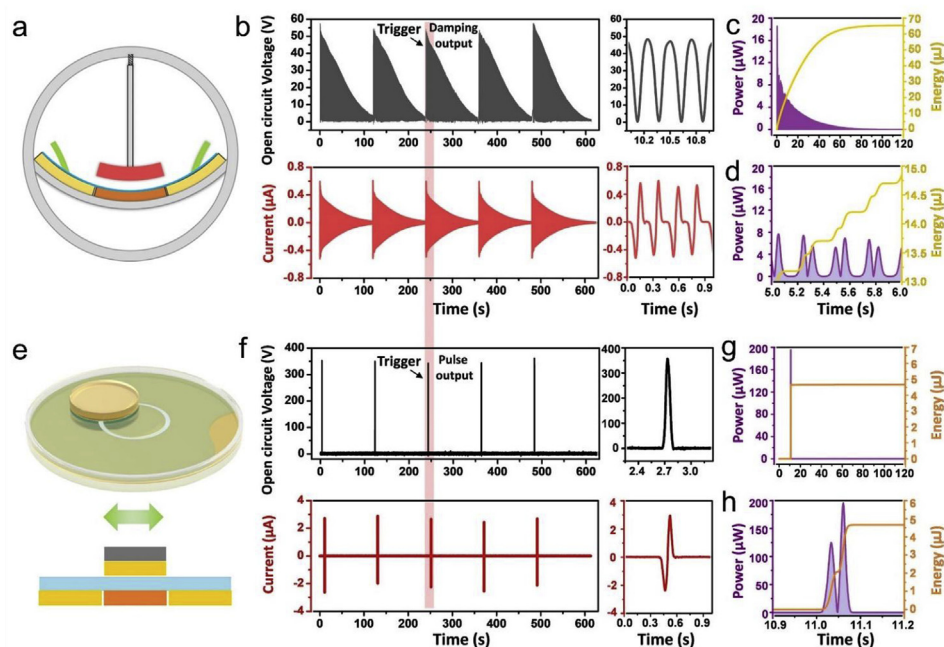


Fig. 3. Comparison of the P-TENG and conventional free-standing TENG. (a) Schematic of the P-TENG. (b) The open-circuit voltage and short-circuit current of the P-TENG by applied an external trigger every 120 s. (c) Output power and converted energy for a trigger. (d) Enlarge view of the output power and converted energy. (e) Schematic of the conventional TENG. (f) Open-circuit voltage and short-circuit current of the conventional free-standing TENG by applied an external trigger every 120 s. (g) Output power and converted energy for a trigger. (h) Enlarge view of the output power and converted energy.

structure without any frictional resistance.

To present a direct comparison of the capability for energy harvesting, we tested the maximum instantaneous peak power ($P = I^2R$) at each matched resistance, as demonstrated in Fig. 3c, g. The peak power of in-plane TENG can reach up to 195.6 μW , and only an optimum output power of 18.6 μW is delivered at a resistance of 90 $\text{M}\Omega$ for the P-TENG (see Supplementary Fig. S3). However, the P-TENG presents an extra power output before the next trigger due to the frequency-multiplied output performance, which largely improves the energy collection efficiency. Moreover, the generated electrical energy obtained at a certain resistance can be calculated by

$$E = \int I(t)^2 \cdot R \cdot dt \quad (2)$$

where, $I(t)$ is the instantaneous current at a certain resistance and R is the load resistance. Fig. 3c, g also show the calculated electrical energy for an external trigger (blue line). The electrical energy generated by the P-TENG increases continuously over time and achieving the value of 65.4 μJ , ultimately. Meanwhile, in-plane TENG can only scavenge the mechanical energy of 4.6 μJ corresponding to one external trigger. That is, the capability of the P-TENG as a sustainable power source is 14.2 times compared with the conventional free-standing TENG, indicating an outstanding energy harvesting ability. The high energy conversion efficiency can be attributed to the pendulum structure without any frictional resistance, which is considered an innovative advantage of this design.

2.4. Performances of the P-TENG

To comprehensively grasp the behavior of the P-TENG, a series of electrical outputs were systematically investigated including different excitation frequencies, directions, and durability. To begin with, a linear motor was employed as external excitation to provide various triggers, as depicted in Fig. 4a–c. The P-TENG shows excellent energy harvesting ability for the low-frequency excitation. Especially, the P-TENG works at a frequency of 0.017 Hz with a smallest voltage of 18.7 V. As with the charges, there is a distinct reduction in the transferred charges as it works, and the transferred charge can achieve 18.2 nC. We also used the P-TENG to charge a capacitor of 2.2 μF to get a reliable comparison of the output power, which indicates a similar trend, and charging rate increases with the elevation of the frequency,

as demonstrated in Fig. 4d, indicating that the proposed P-TENG have excellent energy harvesting performance at low operation frequency. The performance of the P-TENG to charge different capacitors also show a good energy harvesting ability (see Supplementary Fig. S4). Interestingly, we tested output performance of the P-TENG without thin stripes (i.e., no tribo-electrification process exists in such structure), as demonstrated in Supplementary Fig. S5. The values of transferred charges and current are very small, because a very small amount of charges may be generated by the tribo-electrification process happening with air. Furthermore, we tested the capability of energy harvesting for the P-TENG along the arbitrary direction, as depicted in Fig. 4e and f. It is clear that the open-circuit voltage, the short-circuit currents, and peak power stimulated at different angles have the same output values (see Supplementary Fig. S6). To further verify the capability of energy harvesting along an arbitrary direction, the P-TENG was used to charge a capacitor of 3.3 μF , showing the same charging rate at different excitation angles, as demonstrated in Supplementary Fig. S7. These experimental results reveal that the output performance was achieved along a random direction due to the centrosymmetric structure.

The mechanical durability is a superior feature of the P-TENG, which is of paramount importance for energy harvesting practical applications. We carried out the durability tests of the P-TENG, as shown in Fig. 4g, and Supplementary Fig. S8. The output voltage and current amplitudes exhibit negligible changes after a total of 1,000,000 cycles, exhibiting excellent robustness, stability, and durability of the P-TENG. The super durability of the P-TENG is mainly attributed to the innovative structural design, there exists less direct physical contact between the triboelectric layer and the electrodes, so that little damage would be caused on the surface of materials. The durability of the P-TENG was also evaluated by monitoring the surface material abrasion of the PTFE nanowire structures over a long time of work, as demonstrated in Fig. 4h. The scanning electron microscopy (SEM) images of the nanostructured PTFE thin films stayed almost intact for 1,000,000 working cycles.

2.5. Applications of the P-TENG

For large-scale energy harvesting, the P-TENGs were fabricated and organized into an array, as illustrated in Fig. 5a. Since the output phase is different among each unit, every unit is individually rectified then

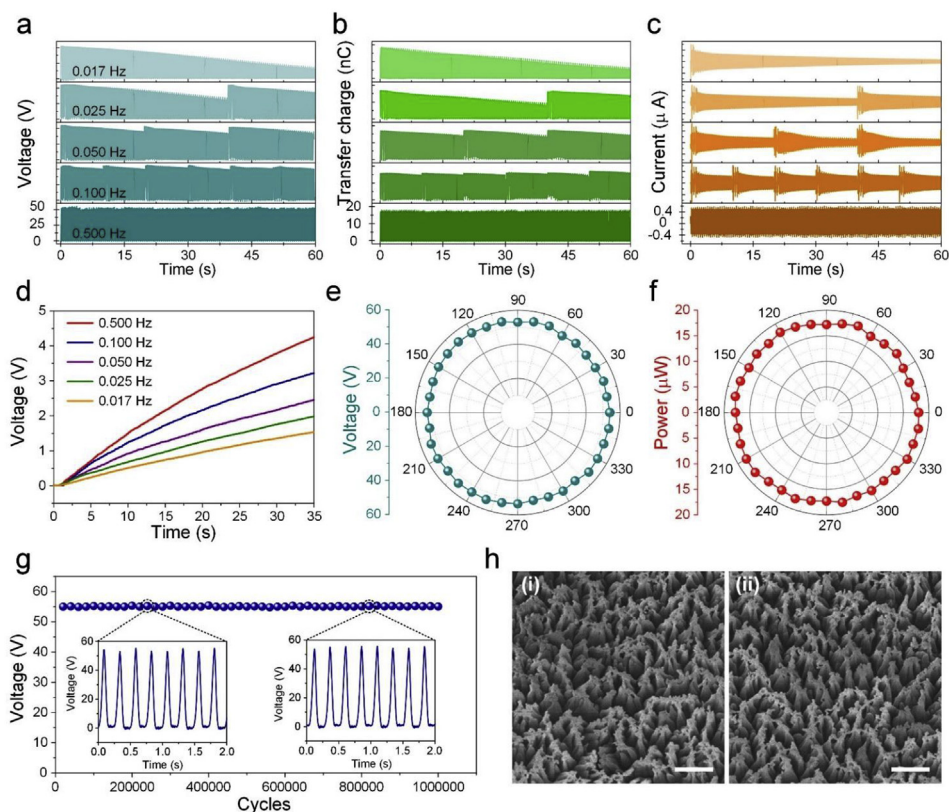


Fig. 4. Performances of the P-TENG. (a) Open-circuit voltage, (b) transferred charge and (c) short-circuit current of the P-TENG at various excitation frequencies. (d) Charging performance of the P-TENG for a $2.2 \mu\text{F}$ capacitor with various frequencies. (e) The output voltage and (f) peak power of the P-TENG simulated from different angles. (g) Durability of the P-TENG over various cycles. (h) Comparison of the surface morphology of the PTFE thin stripes before and after 1,000,000 cycles.

parallelly connected to power the electronics. To explore the output behaviors of the P-TENG array with different unit numbers, we tested the output currents of the P-TENG arrays depending on the number of integrated units, as depicted in Fig. 5b. The output current increases linearly as the increase of unit number, and the maximum current could come up to $3.4 \mu\text{A}$ for six parallel installed units. And the charging performance for different unit was also illustrated that the charging rate increases with the elevation of unit number, as demonstrated in Fig. 5c. Water wave energy is regarded as one of the most prospective renewable energy sources, harvesting wave energy by TENGs would be an ideal method for realizing a self-powered sensing network. A schematic illustration of the configuration of the P-TENG array for wave energy harvesting is shown in Fig. 5d. Thousands of single units were parallelly connected forming a community, which could effectively increase the

output current. Therefore, wave tank experiment was carried out to measure a 2×3 P-TENG array as a power source, which was capable of driving a thermometer to monitor the temperature of the water, as illustrated in Fig. 5e and Supplementary Video S2. It took 780 s for the 2×3 P-TENG array to charge the $100 \mu\text{F}$ capacitor from 0 to 3.1 V and realizing the self-powered temperature sensing, as depicted in Fig. 5f.

Supplementary video related to this article can be found at <https://doi.org/10.1016/j.nanoen.2019.103908>.

Since wind energy is widely distributed in our world, especially in the desert. Harvesting wind energy is a promising solution to generate power. As depicted in Fig. 6a, a series of the P-TENGs were hung on the tree branches to scavenge abundant wind energy in the desert. To begin with, we tested the maximum electric output of the P-TENG as a function of the wind speed simulated by the transient wind, as shown in

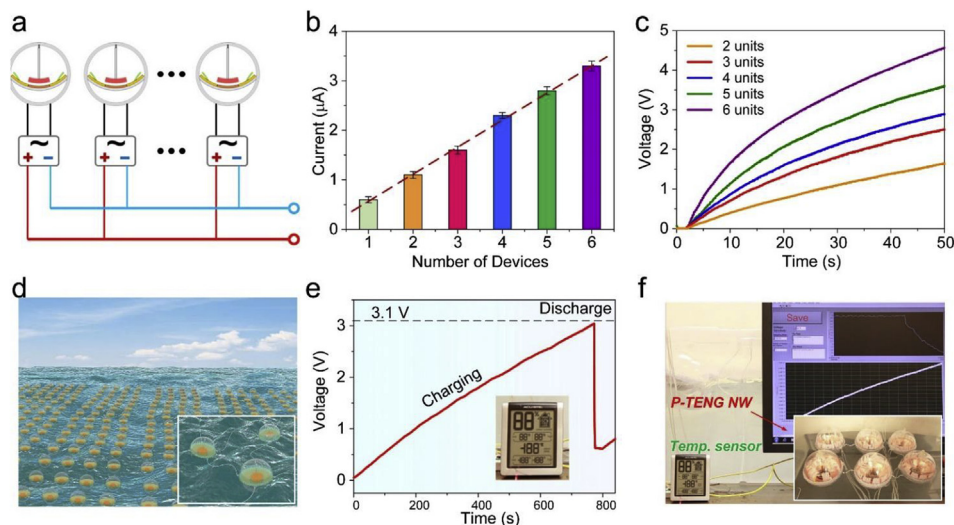


Fig. 5. Output characterization of P-TENG arrays in water for blue energy. (a) Schematic diagram of the rectification circuit for the array. (b) Peak short-circuit current with different amount of integrated units. (c) Charging performance of the P-TENG with different amount of integrated units. (d) Imaginary picture of future large-scale TENG networks for harvesting water wave blue energy. (e) Charging and discharging processes for a capacitor of $100 \mu\text{F}$ to power the thermometer. (f) Photograph of the P-TENG array to power a thermometer.

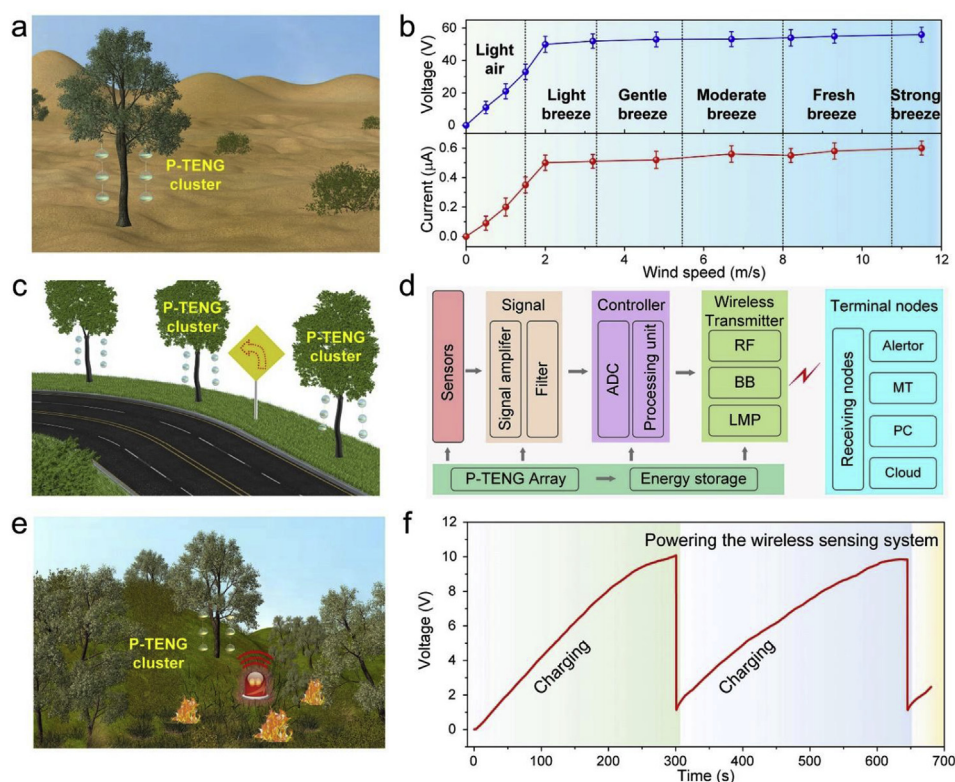


Fig. 6. Wind energy harvesting. (a) Schematic diagram of the P-TENG clusters for harvesting the wind energy in the desert. (b) The output voltage of the P-TENG as a function of the wind speed. (c) Schematic diagram of the P-TENG clusters powering the LEDs as a traffic light. (d) System diagram of a P-TENG-based self-powered wireless forest fire warning system. (e) Schematic diagram of the self-powered wireless forest fire warning system. (f) Charging and discharging processes of the P-TENG clusters for the wireless forest fire warning system.

Fig. 6b. In low wind speed region (< 2 m/s), well-behaved liner variation in the output voltage with wind speed gives a superior sensitivity. As the wind speed is larger than 2 m/s, the output voltage of the P-TENG contains the maximum value around 56 V. That is, the P-TENG is very sensitive to the wind speed due to the pendulum structural design and even the light breeze of wind can make the P-TENG work with the best output performance, which is superior to the electromagnetic generator operating at high wind speed. Various applications of the P-TENG array in wind energy harvesting have been illustrated. **Fig. 6c** demonstrated the P-TENGs hung on the trees, which was used to power light emitting diodes (LEDs) as the traffic light. As a light wind passed by, Traffic light “turn left” can be lighted up by the P-TENGs (see Supplementary Video S3), forming a self-powered traffic indication system. More importantly, an integrated self-powered wireless forest fire warning system was built with P-TENGs for wind energy scavenging, sensors for signals collection and circuits for signal processing and transmission, as the system diagram elucidated in **Fig. 6d**. The power harvested from wind energy was employed to drive the temperature sensor, optimized signal processing, and wireless transmission units. The temperature sensor could monitor the temperature information in the forest and processed by micro-controller, as the schematic diagram shown in **Fig. 6e**. When the temperature increases to the early warning value, the warning information will be sent to the remote terminals, and an alarm lamp will be activated simultaneously, as illustrated in **Supplementary Fig. S9** and **Supplementary Video S4**. **Fig. 6f** depicted the charging and discharging processes for the self-powered wireless forest fire warning system. This creative application would provide new opportunities in real-time remote environment monitoring and the emergency medical system.

Supplementary video related to this article can be found at <https://doi.org/10.1016/j.nanoen.2019.103908>.

3. Conclusions

In summary, we reported a pendulum inspired TENG with frequency-multiplied output and excellent durability as a sustainable and

practical power source. Creatively utilizing thin strip serving as a charge pump, the pendulum triboelectric layer could be replenished charges for electrostatic induction. Taking fully the advantage of the pendulum model, the P-TENG is capable of frequency-multiplied output performance, achieving a remarkable energy harvesting efficiency. Owing to the pendulum structural design with an air gap between triboelectric layer and electrodes, the P-TENG works at the free-standing mode without any frictional resistance, which is contributed to the superior device robustness and durability. A systematical investigation of the dependence of performance on the frequencies and the directions were comprehensively explored. Moreover, the P-TENG array was adopted to scavenge water wave energy and wind energy for driving electronics, which presents a possible green and effective route to large-scale energy harvesting. Given such features of the frequency-multiplied output, excellent durability, sensitive to excitation, and trigger by random directions, the P-TENG presented in this work is a practical approach in scavenging mechanical energy for self-powered sensing system as well as possibly for generating electricity at a large scale.

4. Experimental section

4.1. Fabrication of the pendulum inspired TENG

For the electrode layer, an acrylic spherical shell with an inner diameter of 130 mm was tailored by laser cutting (PLS6.75, Universal Laser Systems) to form a cambered acrylic with a circular diameter of 120 mm as the substrate. Then a circular copper film and a ring copper film were adhered on the surface of the cambered acrylic as the electrodes. A piece of PTFE film (with a thickness of 100 µm) was adhered to the electrodes as the dielectric layer. For the thin stripes, a piece of PTFE film was processed by laser cutter into 3 mm × 20 mm rectangular stripes, which were uniformly fixed at the edge of the cambered acrylic as the charge pump. For pendulum triboelectric layer, another acrylic spherical shell with an inner diameter of 130 mm was cut into a cambered acrylic with a circular diameter of 35 mm as the pendulum substrate. A copper film was adhered on the surface of such cambered

acrylic as the pendulum triboelectric layer. And an acrylic rod with the length of 62 mm was vertically fixed with the pendulum substrate as the pendulum rod. Then the acrylic rod was connected to the outer acrylic spherical shell (inner diameter: 120 mm) with a nylon rope for free oscillation. Finally, the outer acrylic spherical shell is sealed by the sealant to shielding the effect of water vapor or charged particles that exist in air to the triboelectric charges.

4.2. Characterization and measurements

For the measurements of the P-TENG, the external excitation was applied by a linear motor, and a programmable electrometer (Keithley 6514) was used to measure the open-circuit voltage and transferred charge, a low-noise current preamplifier (model no. SR570) was adopted to test the short-circuit current. The wind was produced by a commercial air gun, and wind speed was tested via a commercial anemometer.

Author contributions

Z.L., B.Z., H.G. and Z.L.W. conceived the idea, analysed the data and wrote the paper. Z.L., B.Z., Z.W., and H.Z. fabricated the P-TENG and did electric measurement. H.G. and J.Y. optimized the structure of the P-TENG. H.Z. helped with the manuscript. All the authors discussed the results and commented on the manuscript.

Competing interests

The authors declare no competing financial interests.

Acknowledgements

The authors acknowledge support from National Natural Science Foundation of China (NSFC No. 51576161), and 111 project (B16038). Z.L. thanks China Scholarship Council for supplying oversea scholarship.

Appendix A. Supplementary data

Supplementary data to this article can be found online at <https://doi.org/10.1016/j.nanoen.2019.103908>.

References

- [1] W. Gao, S. Emaminejad, H.Y.Y. Nyein, S. Challa, K.V. Chen, A. Peck, H.M. Fahad, H. Ota, H. Shiraki, D. Kiriya, D.H. Lien, G.A. Brooks, R.W. Davis, A. Javey, Fully integrated wearable sensor arrays for multiplexed in situ perspiration analysis, *Nature* 529 (2016) 509–514.
- [2] Q. Jing, Y. Xie, G. Zhu, R.P.S. Han, Z.L. Wang, Self-powered thin-film motion vector sensor, *Nat. Commun.* 6 (2015) 8031.
- [3] X. Pu, H. Guo, J. Chen, X. Wang, Y. Xi, C. Hu, Z.L. Wang, Eye motion triggered self-powered mechnosensational communication system using triboelectric nanogenerator, *Sci. Adv.* 3 (2017) e1700694.
- [4] H.H. Chou, A. Nguyen, A. Chortos, J.W.F. To, C. Lu, J.G. Mei, T. Kurosawa, W.G. Bae, J.B.H. Tok, Z.A. Bao, A chameleon-inspired stretchable electronic skin with interactive colour changing controlled by tactile sensing, *Nat. Commun.* 6 (2015) 8011.
- [5] J. Yang, J. Chen, Y. Su, Q. Jing, Z. Li, F. Yi, X. Wen, Z. Wang, Z.L. Wang, Eardrum-inspired active sensors for self-powered cardiovascular system characterization and throat-attached anti-interference voice recognition, *Adv. Mater.* 27 (2015) 1316–1326.
- [6] Y. Lee, S.H. Cha, Y.W. Kim, D. Choi, J.Y. Sun, Transparent and attachable ionic communicators based on self-cleanable triboelectric nanogenerators, *Nat. Commun.* 9 (2018) 1804.
- [7] H.Y. Guo, X.J. Pu, J. Chen, Y. Meng, M.H. Yeh, G.L. Liu, Q. Tang, B.D. Chen, D. Liu, S. Qi, C.S. Wu, C.G. Hu, J. Wang, Z.L. Wang, A highly sensitive, self-powered triboelectric auditory sensor for social robotics and hearing aids, *Sci. Robot* 3 (2018) eaat2516.
- [8] Z.L. Wang, J.H. Song, Piezoelectric nanogenerators based on zinc oxide nanowire arrays, *Science* 312 (2006) 242–246.
- [9] V. Nguyen, S. Kelly, R. Yang, Piezoelectric peptide-based nanogenerator enhanced by single-electrode triboelectric nanogenerator, *Apl. Mater.* 5 (2017) 074108.
- [10] H. Yuan, T. Lei, Y. Qin, R. Yang, Flexible electronic skins based on piezoelectric nanogenerators and piezotronics, *Nano Energy* 59 (2019) 84–90.
- [11] Y. Qin, X. Wang, Z.L. Wang, Microfibre-nanowire hybrid structure for energy scavenging, *Nature* 451 (2008) 809–813.
- [12] L.E. Bell, Cooling, heating, generating power, and recovering waste heat with thermoelectric systems, *Science* 321 (2008) 1457–1461.
- [13] D. Kraemer, B. Poudel, H.P. Feng, J.C. Taylor, B. Yu, X. Yan, Y. Ma, X.W. Wang, D.Z. Wang, A. Muto, K. McEnaney, M. Chiesa, Z.F. Ren, G. Chen, High-performance flat-panel solar thermoelectric generators with high thermal concentration, *Nat. Mater.* 10 (2011) 532–538.
- [14] S. Niu, X. Wang, F. Yi, Y.S. Zhou, Z.L. Wang, A universal self-charging system driven by random biomechanical energy for sustainable operation of mobile electronics, *Nat. Commun.* 6 (2015) 8975.
- [15] G. Zhu, J. Chen, T. Zhang, Q. Jing, Z.L. Wang, Radial-arrayed rotary electrification for high performance triboelectric generator, *Nat. Commun.* 5 (2014) 3426.
- [16] J.M. Donelan, Q. Li, V. Naing, J.A. Hoffer, D.J. Weber, A.D. Kuo, Biomechanical energy harvesting: generating electricity during walking with minimal user effort, *Science* 319 (2008) 807–810.
- [17] Y. Qi, M.C. McAlpine, Nanotechnology-enabled flexible and biocompatible energy harvesting, *Energy Environ. Sci.* 3 (2010) 1275–1285.
- [18] Y. Qi, J. Kim, T.D. Nguyen, B. Lisko, P.K. Purohit, M.C. McAlpine, Enhanced piezoelectricity and stretchability in energy harvesting devices fabricated from buckled PZT ribbons, *Nano Lett.* 11 (2011) 1331–1336.
- [19] F.R. Fan, Z. Tian, Z.L. Wang, Flexible triboelectric generator!, *Nano Energy* 1 (2012) 328–334.
- [20] J. Yang, J. Chen, Y. Yang, H. Zhang, W. Yang, P. Bai, Y. Su, Z.L. Wang, Broadband vibrational energy harvesting based on a triboelectric nanogenerator, *Adv. Energy Mater.* 4 (2014) 1301322.
- [21] Z. Lin, J. Chen, X. Li, Z. Zhou, K. Meng, W. Wei, J. Yang, Z.L. Wang, Triboelectric nanogenerator enabled body sensor network for self-powered human heart-rate monitoring, *ACS Nano* 11 (2017) 8830–8837.
- [22] J. Wang, S. Li, F. Yi, Y. Zi, J. Lin, X. Wang, Y. Xu, Z.L. Wang, Sustainably powering wearable electronics solely by biomechanical energy, *Nat. Commun.* 7 (2016) 12744.
- [23] H. Zou, Y. Zhang, L. Guo, P. Wang, X. He, G. Dai, H. Zheng, C. Chen, A.C. Wang, C. Xu, Z.L. Wang, Quantifying the triboelectric series, *Nat. Commun.* 10 (2019) 1427.
- [24] Z. Lin, J. Yang, X. Li, Y. Wu, W. Wei, J. Liu, J. Chen, J. Yang, Large-scale and washable smart textiles based on triboelectric nanogenerator arrays for self-powered sleeping monitoring, *Adv. Funct. Mater.* 28 (2018) 1704112.
- [25] J. Chen, Z.L. Wang, Reviving vibration energy harvesting and self-powered sensing by a triboelectric nanogenerator, *Joule* 1 (2017) 480–521.
- [26] C. Xu, Y. Zi, A.C. Wang, H. Zou, Y. Dai, X. He, P. Wang, Y.C. Wang, P. Feng, D. Li, Z.L. Wang, On the electron-transfer mechanism in the contact-electrification effect, *Adv. Mater.* 30 (2018) 1706790.
- [27] W. Liu, Z. Wang, G. Wang, G. Liu, J. Chen, X. Pu, Y. Xi, X. Wang, H. Guo, C. Hu, Z.L. Wang, Integrated charge excitation triboelectric nanogenerator, *Nat. Commun.* 10 (2019) 1426.
- [28] Z. Lin, Z. Wu, B. Zhang, Y.-C. Wang, H. Guo, G. Liu, C. Chen, Y. Chen, J. Yang, Z.L. Wang, A triboelectric nanogenerator-based smart insole for multifunctional gait monitoring, *Adv. Mater. Technol.* 4 (2018) 1800360.
- [29] Y. Chen, Y.C. Wang, Y. Zhang, H. Zou, Z. Lin, G. Zhang, C. Zou, Z.L. Wang, Elastic-beam triboelectric nanogenerator for high-performance multifunctional applications: sensitive scale, acceleration/force/vibration sensor, and intelligent keyboard, *Adv. Energy Mater.* 8 (2018) 1802159.
- [30] Z. Zhou, X. Li, Y. Wu, H. Zhang, Z. Lin, K. Meng, Z. Lin, Q. He, C. Sun, J. Yang, Z.L. Wang, Wireless self-powered sensor networks driven by triboelectric nanogenerator for in-situ real time survey of environmental monitoring, *Nano Energy* 53 (2018) 501–507.
- [31] G. Liu, J. Chen, Q. Tang, L. Feng, H. Yang, J. Li, Y. Xi, X. Wang, C.G. Hu, Wireless electric energy transmission through various isolated solid media based on triboelectric nanogenerator, *Adv. Energy Mater.* 8 (2018) 1703086.
- [32] L. Lin, Y. Xie, S. Niu, S. Wang, P. Yang, Z.L. Wang, Robust Triboelectric nanogenerator based on rolling electrification and electrostatic induction at an instantaneous energy conversion efficiency of similar to 55%, *ACS Nano* 9 (2015) 922–930.